



Evaluation and analysis of metal mine filling based on numerical simulation and actual measurement

Lifu Pang^{1,2} · Weitao Liu^{1,2} · Qiushuang Zheng^{1,2} · Yanhui Du^{2,3} · Xiangxi Meng^{2,3} · Xin Li⁴

Received: 18 June 2020 / Accepted: 9 July 2021 / Published online: 7 August 2021
© The Author(s), under exclusive licence to Springer-Verlag GmbH Germany, part of Springer Nature 2021

Abstract

In order to make a reasonable evaluation of the effect of backfill mining on non-coal mines, the first phase of the Laixin iron ore mine project is taken as an example. First, a geomechanical model of iron ore mining was established according to geological theory; second, numerical simulation software FLAC3D was used to analyze the surface subsidence, horizontal displacement, plastic failure range of the surrounding rocks, and stress conditions of the surface and surrounding rocks under unfilled and filled conditions; finally, the observation data of surface subsidence in the open area were analyzed against the background of the Phase I mining project of Laixin iron ore mine. The results show that: (1) the amount of surface subsidence increases with the increase of burial depth. As the mining depth increases, the amount of ground subsidence gradually increases. (2) Numerical simulation of the amount of surface subsidence and horizontal displacement in the unfilled condition is ten times that in the filled condition; the plastic zone of destruction in the unfilled condition extends to the surface, and the plastic destruction in the filled condition is mainly in the vicinity of the mining location, and the vertical stress in the unfilled condition is much larger than that in the filled condition; (3) the on-site measured results are basically consistent with the numerical simulation results, and the numerical simulation can be used to reasonably predict the amount of subsidence and horizontal displacement of the ground surface, and the force on the goaf.

Keywords Computational analysis · Numerical simulation · Ground subsidence · Horizontal displacement · Plastic failure · Field observation

Introduction

With the reduction of land resources, the government requires that protective measures should be adopted in the mining process. At present, the use of waste gangue to fill the mining area is a green mining method recognized by the

world (Fu et al. 2014; Feng et al. 2015; Wang et al. 2018). The use of waste gangue to fill the goaf can effectively solve the problem of surface subsidence and movement (Villegas et al. 2011; Qi and Gao 2013; Strozzi et al. 2017). The filling effect is directly related to the quality of the project after filling. Therefore, how to effectively evaluate the filling effect need a lot of research work.

At present, the problem of mine filling is generally divided into coal mine filling and non-coal mine filling. Chen et al. (2017) conducted physicochemical evaluation, proportional strength test, and pumpability test to evaluate the feasibility of mixed construction waste and ultrafine tailings (CW&UT) as underground mine filling aggregates (Dai et al. 2011; Fokker et al. 2012). Deng et al. (2017) used the practice of cemented filling technology of ultra-fine tailings in a gold mine as the background. A series of tests were carried out on the performance of ultrafine filling materials (Li et al. 2015). Li et al. (2017) used an experimental approach to analyze the effect of material particle size on surface sedimentation. Yin et al. (2018) used sulphide mine tailings as

✉ Lifu Pang
plf1715@163.com

¹ College of Energy and Mining Engineering, Shandong University of Science and Technology, Qingdao 266590, Shandong, China

² Shandong University of Science and Technology State Key Laboratory of Mine Disaster Prevention and Control, Qingdao 266590, Shandong, China

³ College of Safety and Environmental Engineering, Shandong University of Science and Technology, Qingdao 266590, Shandong, China

⁴ Laiwu Laixin Iron Ore Co., Ltd, Jinan 266590, Shandong, China

raw material to prepare a cement tailings backfill (CTB). They used numerical simulation and combined the backfill formulation (sulfur content, binder dosage, solids concentration) and curing time to analyze the expansion performance of the filler. Sun et al. (2018) used theoretical analysis and numerical simulation (FLAC 3D) to determine the coal pillars and mining width in order to ensure the safety of the coal pillars and improve the recovery coefficient, and discussed the stress distribution and surface settlement of the coal pillars under different mining conditions. Chen et al. (2019) used modeling to evaluate the mechanical and operational properties of the filler. Ouattara et al. (2017) studied the rheological properties of cement paste backing (CPB) in the field, which influenced the flow characteristics of the filler during transportation in an open pit. Chaussard and Kerosky (2016) use optical satellite data to identify legal and illegal mining sites, monitor on-site black sand mining activities and characterize the direct impact of mining on the landscape (Lin et al. 2018; Juncosa et al. 2019). Strozzi et al. (2011) used ENVISAT ASAR data to detect significant deformations of 1–12 mm/year above the tunnels on villages and sparsely vegetated alpine slopes to simulate the expected surface deformation before and during construction (Lu et al. 2017). Lee et al. (2012) used field experiments to hydraulically fill fly ash by establishing an inclined well, and evaluated the filling effect (Emad et al. 2018). Li et al. (2020) used laboratory tests to evaluate the filling materials. The above scholars have all analyzed the filling effect from a single perspective (Cai et al. 2015; Ma et al. 2020). In order to evaluate the filling effect more reasonably and effectively, this paper evaluates the filling effect of the Laixin iron ore mine using a combination of model building, theoretical calculation, numerical simulation and field measurements.

Geomechanical model and calculation of subsidence

Geomechanical models

The main ore body of Laixin iron ore is buried at a depth of -300 m to -500 m, and the thickness of the ore body is 20 m. A geological model is established based on geological principles (Fig. 1). When the ore body is initially excavated, the original stress state of the surrounding rock is destroyed and a stress concentration zone appears at the initial location of the ore body excavation. As the ore body is continuously mined, the mining intensity increases, and the ground surface subsides above the goaf. When the ore body is excavated to the limit of full mining, the maximum value of surface subsidence occurs. Based on the knowledge of elastic mechanics, the model of insufficient mining and full mining subsidence is established (Fig. 2).

Where H_0 (°) is the mining depth, m; α is the full-mining angle; L (m) is the directional mining dimension; w_1 (m) and w_2 (m) are the maximum ground subsidence values under insufficient mining and full mining conditions, respectively.

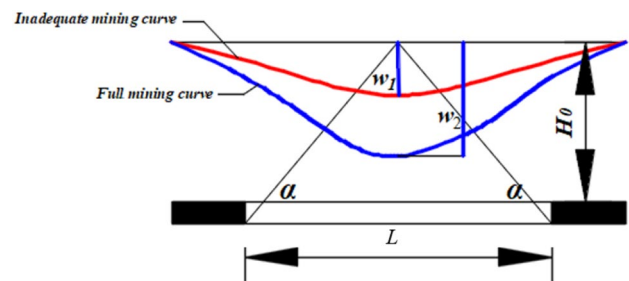


Fig. 2 Under-mining and fully mining subsidence models

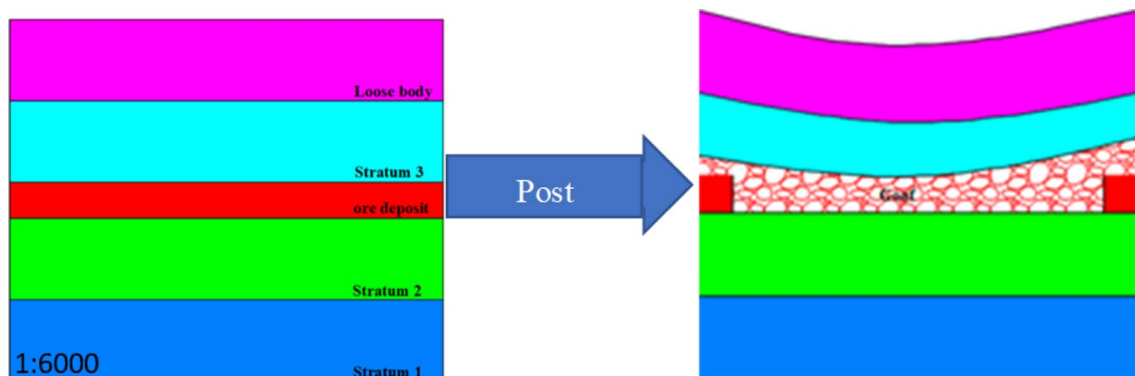


Fig. 1 Geological model of mining

Fig. 3 Sinking model

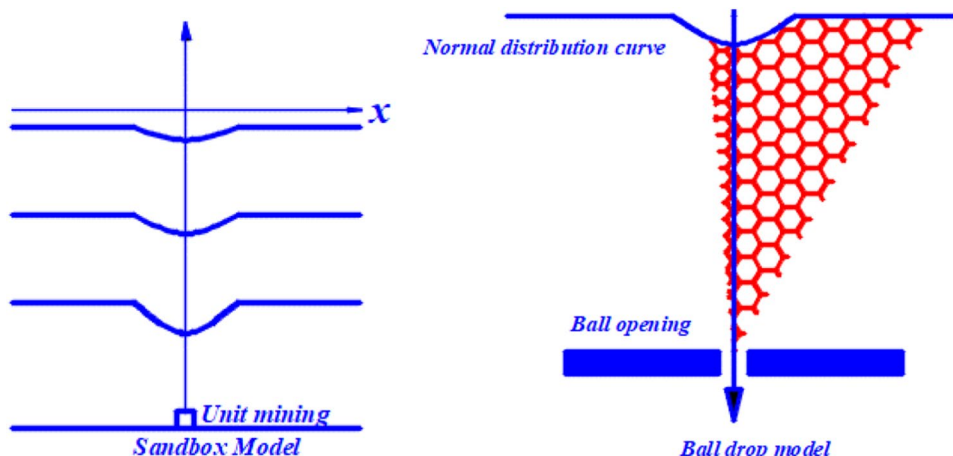
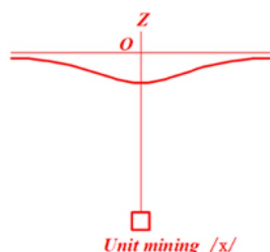


Fig. 4 Unit sinking basin



Prediction and calculation of surface subsidence

Surface subsidence prediction calculations using probabilistic integration method. For surface subsidence after iron ore mining, a sandbox model and a ball-fall model (Fig. 3) can be developed to illustrate the subsidence. The sinking curve presented by this model is similar to the probability distribution density curve of a normal distribution.

Regarding the mining method of iron ore, it can be regarded as unit mining. Unit mining will form a unit sinking basin (Fig. 4). The sinking curve of the unit sinking basin is a normal distribution curve. The shape of the curve is consistent with the density curve of the probability distribution of rock subsidence.

The stable unit sinking basin expression is obtained by derivation:

$$W_e = \frac{h}{\sqrt{\pi}} \cdot e^{-h^2 x^2}, \tag{1}$$

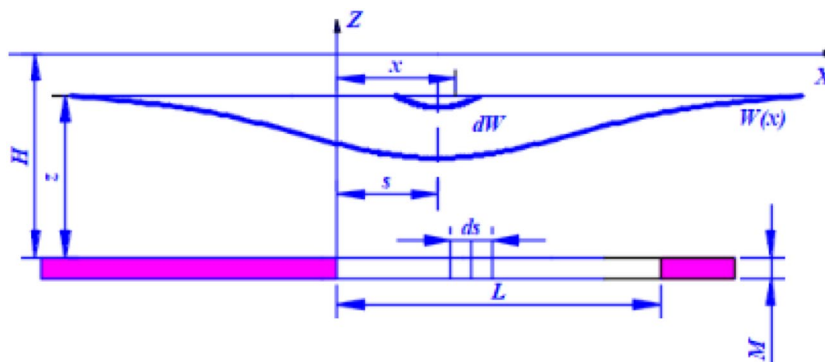
where h (m) is constant; W_e (m) is sinking distance; x (m) is the displacement of the basin along the X direction.

The surface subsidence model is established for the mining area of Laishin iron ore (Fig. 5). The Z -axis is located at the initial position of excavation, Z is the level of any height, and when it reaches the surface, it is the mining depth H . The origin O is the intersection of the vertical axis and the ore level. The X -axis, along the surface level, is the X -direction of the shifting basin at the surface.

Assuming that the ore is buried in depth H (m), the ore thickness is M (m), and the distance from the origin O is s in the ore body. The width of the extracted ore body is ds , above which a small subsidence basin dW is initially formed at level z . From the expression for the unit basin, the subsidence caused by ds is obtained:

$$dW = qM \frac{H}{\sqrt{\pi}} e^{-H^2(x-s)^2} ds, \tag{2}$$

Fig. 5 Rock settlement under the influence of arbitrary mining in Laixin Iron Mine



where q is subsidence coefficient.

According to the superposition principle, when the mining width is L , that is, under any mining conditions, the following formula is available:

$$W_{(s)} = qM \frac{H}{\sqrt{\pi}} \int_0^L e^{-H^2(x-s)^2} ds. \quad (3)$$

For a semi-infinite basin, when $L \rightarrow \infty$, Eq. (4) is shown below:

$$W_{(s)} = qM \frac{H}{\sqrt{\pi}} \int_0^{\infty} e^{-H^2(x-s)^2} ds. \quad (4)$$

According to Eq. (4), we can calculate the amount of subsidence of the ground surface or rock layer at any initial time. It is known that the mining depths of the Laixin iron ore are $H = -310$ m, -410 m, -510 m, and the thickness of the mining bodies are 11 m, 10 m, and 12 m, respectively. According to the research of Li Hailiang et al. (2014), the subsidence coefficient q is 0.6, and the impact of mining cannot reach an infinite range. Therefore, L is 2000 m, X is 500 m, and $0 < s < 50$ m. MATLAB software is used to process the data, so the subsidence curve at different mining depths can be obtained (Fig. 6).

Figure 6 shows that no subsidence occurred at the beginning of mining, and the surface began to be affected when the mining length was about 25 m. As the face length advanced, the surface subsidence increased. In addition, the amount of subsidence on the surface increases. As the mining depth increased, the amount of subsidence at the surface gradually increased, and the maximum subsidence at the -300 m, -400 m, and -500 m levels at about 70 m was 75 mm, 70 mm, and 60 mm, respectively.

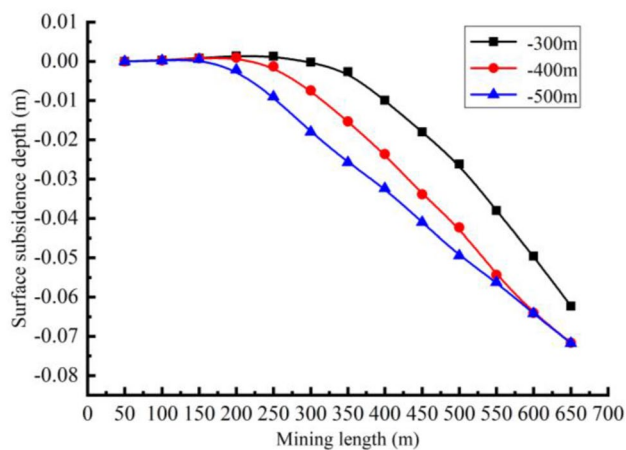


Fig. 6 Subsidence curves for mining at different depths

Numerical simulation

Engineering background

Laiwu Laixin Iron Mine is located in Niuquan Town, Laiwu City, Shandong Province, which is 12 km away from Laiwu City in the east and 7.5 km away from Xintai Railway Linjialou Station in the north, with convenient transportation. The region has a warm temperate continental climate with an extreme maximum temperature of 39.2 °C and an extreme minimum temperature of -21.8 °C. The average annual precipitation is 766.4 mm, the average annual wind speed is 3.0 m/s, and the predominant wind direction is northeast throughout the year. The seismic intensity is 7°. The mine site is covered with farmland, with Ji Jia Zhuang and Xi Shang Zhuang to the south and west, respectively (the nearest distance between the mine site and the village is 500–600 m). The environmental quality is good, as there are almost no other industries in the area except for the Laixin iron ore mine. There is no nature reserve or cultural relic reserve in the vicinity.

Laixin Iron Mine is a limited liability company controlled by Luzhong Metallurgical Mining Group. The mine has six ore belts and 16 ore bodies, with a total resource of 44.09 million tons submitted in the geological investigation report, of which 8.98 million t of geological reserves are mined in the first phase. The second phase of the project is planned to mine three ore bodies above -305 m in the eastern ore zone IV, V, and three ore bodies between -305 m and -505 m in the western ore zone (Fig. 7).

Model establishment

In order to verify the calculated surface subsidence results from the theoretical analysis, we analyze the subsidence displacements, horizontal displacements, and stress conditions of the surface and surrounding rocks in the plastic failure range of the surrounding rocks after filling and mining, and reasonably evaluate the filling effect. This paper uses the finite difference simulation software FLAC3D to perform numerical simulation of ore body excavation. FLAC 3D (Fast Lagrangian Analysis of Continua) simulation computing software developed by American ITASCA.

According to the actual geological conditions and mining parameters of Laixin iron ore mine and the characteristics of the roof and floor rocks, the height range (Z direction) of the model is from -100 to -500 m, and the length and width are 400 m, respectively. The strength reduction method is used to simplify the relevant parameters and establish the model. The scale in the figure is all 1:6000, that is, 1 cm in the figure is roughly equal to

Fig. 7 Location map



Table 1 Material performance parameters

Parameter	Surrounding rock	Mineral	Filling body
Gravity (t/m^3)	2.8	3	2.5
Bond strength (MPa)	1.8	1.8	0.7
Internal friction angle ($^\circ$)	39	38	36
Tensile strength (MPa)	1.1	0.7	0.6
Elastic modulus (MPa)	16,000	14,000	7000
Poisson's ratio	0.17	0.32	0.19

60 m in reality. The model is divided into 67,200 hexahedral units and 72,283 nodes. The boundaries of the model are horizontally constrained, the upper boundary is free, and the bottom boundary is fully constrained. Two simulation scenarios are carried out, without filling and with filling. The excavation is 20 m at each step along the strike length, and 15 steps are excavated, totaling 300 m. For the geological conditions of the Laishin Mine, the numerical simulation treats the media with different mechanical properties, such as the filling body, ore body and surrounding rock, as isotropic elasto-plastic continuous media, and the yield conditions adopt the Moore–Cullen criterion. The mechanical parameters of the selected ore body, filling body and surrounding rock are shown in Table 1. A three-dimensional numerical analysis model of FLAC3D (Fig. 8) was established based on the above conditions. The mining scheme under unfilled conditions was used as a comparison.

Simulation scenario design

After the model is established, in order to monitor and record the subsidence and horizontal displacement of each layer of the surface and roof strata in the simulation process, the coordinate points in Table 2 are selected for monitoring.

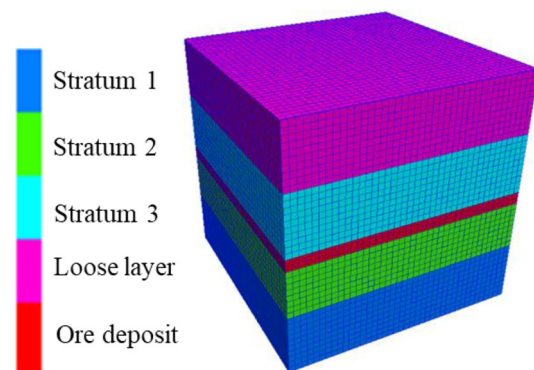


Fig. 8 Three-dimensional numerical analysis model

In $Z=250$, $Z=300$, $Z=350$, $Z=400$ layers, respectively, 5 coordinates are selected for every 50 m height, and 20 coordinates are taken for 4 layers. The schematic diagram of selecting points is shown in Fig. 9. In the simulation process, the 101–120 point subsidence displacement and horizontal displacement were recorded separately. In order to distinguish from the subsidence count, the coordinates of the 101–120 point recorded by the horizontal displacement were named 121–140. Consider the displacement along the X direction during the simulation as horizontal displacement.

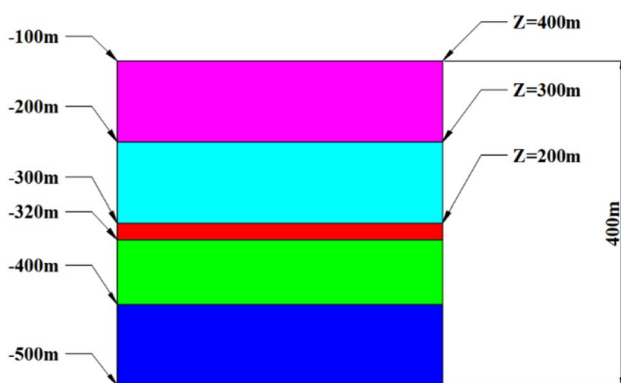
Results analysis

Analysis of subsidence

When an ore body is excavated at different distances, the subsidence of the stratum directly affects the stability of the surface environment. Numerical simulation is used to monitor and record the subsidence of different strata in order to effectively predict the impact of ore body mining on the

Table 2 Data table of different layers

Stratum	Coordinate point	X (m)	Y (m)	Z (m)
Z=250 m	101	100	200	400
	102	150	200	400
	103	200	200	400
	104	250	200	400
	105	300	200	400
Z=300 m	106	100	200	350
	107	150	200	350
	108	200	200	350
	109	250	200	350
	110	300	200	350
Z=350 m	111	100	200	300
	112	150	200	300
	113	200	200	300
	114	250	200	300
	115	300	200	300
Z=400 m	116	100	200	250
	117	150	200	250
	118	200	200	250
	119	250	200	250
	120	300	200	250

**Fig. 9** Schematic diagram of each layer

environment. Because the Laixin iron ore mine adopts the mining method of tailings filling, statistical analysis of the subsidence amount after filling can be used to evaluate the filling effect. For comparison, it is necessary to predict the amount of subsidence during filling as well.

Analysis of the amount of subsidence without filling

The finite difference software FLAC3D was used to simulate the excavation of the ore body without tailings filling, and the subsidence curves at points 101–120 were obtained (Fig. 10). When Fig. 10 was analyzed separately, it was

found that the law of subsidence is consistent in different horizons, and the subsidence increases continuously as the working face advances. The curves in Fig. 10 all show a tendency for the adjacent peaks to gradually increase. The subsidence is negligible in the 50 m range of the excavated ore body, and after 50 m it starts to show a regular increase. Comparing Fig. 10(1)–(4), it can be found that the maximum value of subsidence increases with the increase of burial depth, which is consistent with the results of the theoretical calculation. For the curves within each figure in Fig. 10, it can be found that within the same layer, the peak becomes larger as the value of X increases.

When the mining distance is the same, the amount of subsidence in different layers is also of interest. It is necessary to analyze the amount of subsidence at different layers when the mining distance is the same. The subsidence curves are plotted according to the data obtained from numerical simulations at each point (Fig. 11). According to Fig. 11, it can be seen that the greater the depth of burial, the greater the amount of subsidence under the same advancing distance conditions. Similarly, each of the curves conforms to the pattern of smaller subsidence in the first 50 m of mining, as shown in Fig. 11. As the working face advances, it can be seen that the closer the point to the mining location, the greater the amount of subsidence.

Comprehensive analysis of Figs. 10 and 11, it can be found that the peak values of the maximum subsidence at different depths all exceed 0.3 m. Basically, they all show a broken line state of increasing trend.

Analysis of subsidence during filling

The finite difference software FLAC3D was used to simulate the excavation of the ore body under the tailings filling condition, and the subsidence curves of points 101–120 under the filling condition were obtained (Fig. 12).

According to Fig. 12, under the same stratigraphic conditions, points 105, 110, 115, and 120 all show the law of increasing subsidence with the advancement of the working surface. All other points show a tendency of increasing subsidence before the face advances to 150 m and decreasing subsidence in the range of 150–300 m. This is because the role of the filler is limited in the early stage of mining, and as the fill area increases, the role of the filler in stabilizing the stratum and controlling subsidence becomes greater and greater. Points 105, 110, 115, and 120 are all later stages of mining and are, therefore, affected by mining for longer periods of time and less by the role of the fill body. When the ore body was mined and filled, the amount of subsidence was reduced by a factor of about ten compared to the unfilled level, so it can be considered that the filling effect is good and effectively reduces the amount of subsidence.

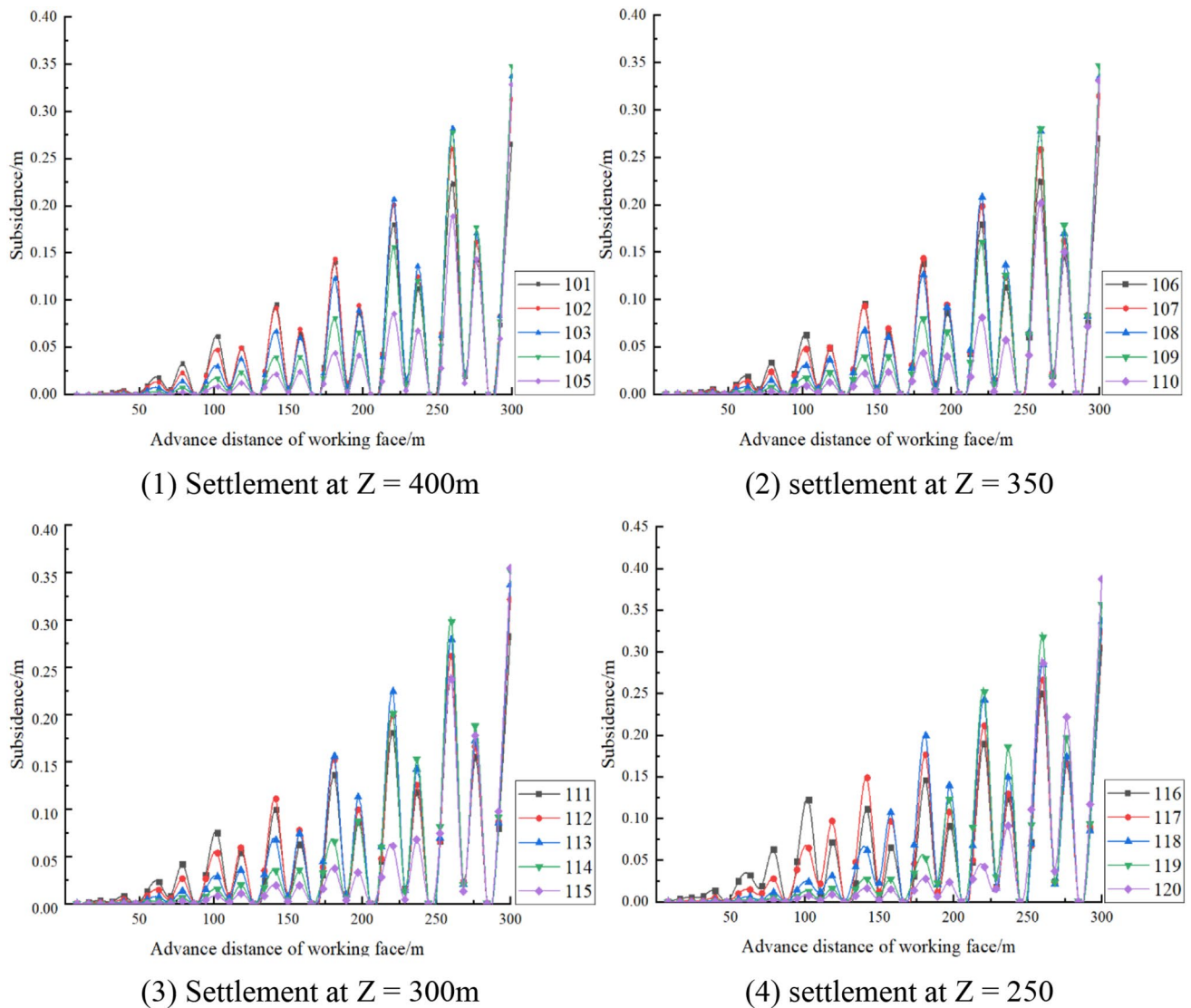


Fig. 10 Different stratum subsidence amounts as the working face advances when unfilled

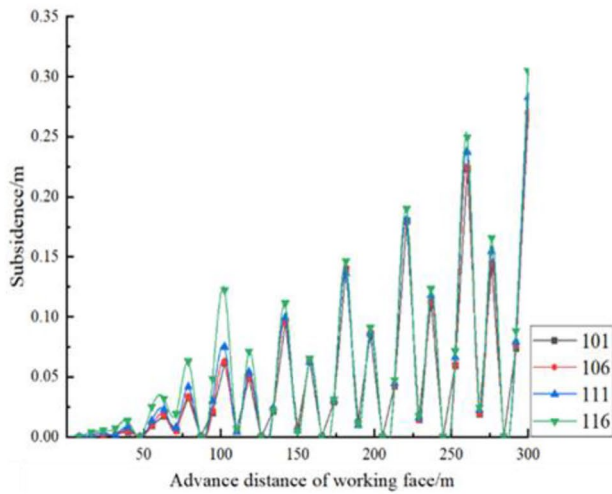
The analysis curves (Fig. 13) of the subsidence amount in different layers with the same value of mining X during mining and filling are shown below. According to Fig. 13, when the value of X is the same, the subsidence at the X mining location is the largest; the closer the mining location is to the sink volume, the larger the sink volume will be, and the sink volume will gradually increase as the burial depth increases.

Horizontal displacement analysis

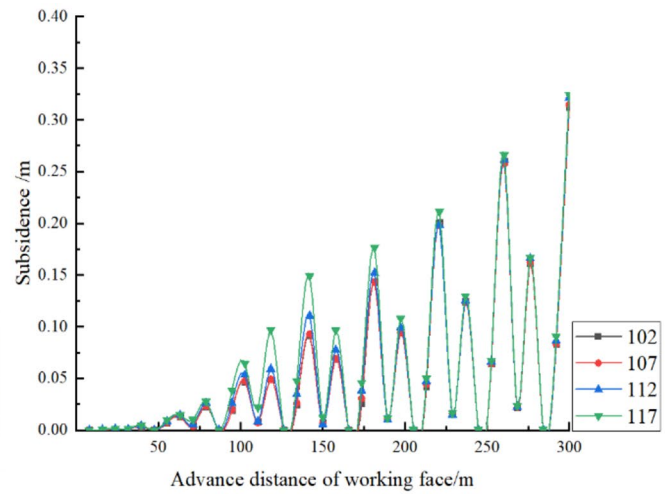
According to some experts and scholars, the impact of horizontal displacements on the earth’s surface cannot be ignored. The rupture of surface structures is largely caused by excessive horizontal displacements. According to the finite difference software FLAC3D, an excavation simulation of the ore body without tailings filling was performed,

and the subsidence curves at points 121–140 were obtained (Fig. 14).

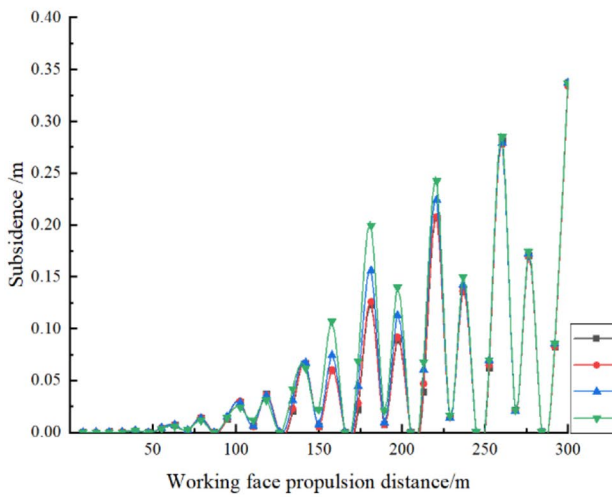
According to Fig. 14(1), the displacement at each point in the horizontal direction gradually increases as the working surface advances. The increase in horizontal displacement is larger in the negative direction and slower in the positive direction along the horizontal plane. At points 121–125 on the surface, the horizontal displacement near the mining position is larger as the mining progresses. The horizontal displacement is greatest at the point, where the face advances to about 250 m. According to Fig. 14(2), at $Z = 350$ m, the horizontal displacement in the negative direction occurs when the face advances to about 150 m, and the horizontal displacement first increases and then decreases as the face advances. In the working surface range of 150–300 m, the horizontal displacement in the



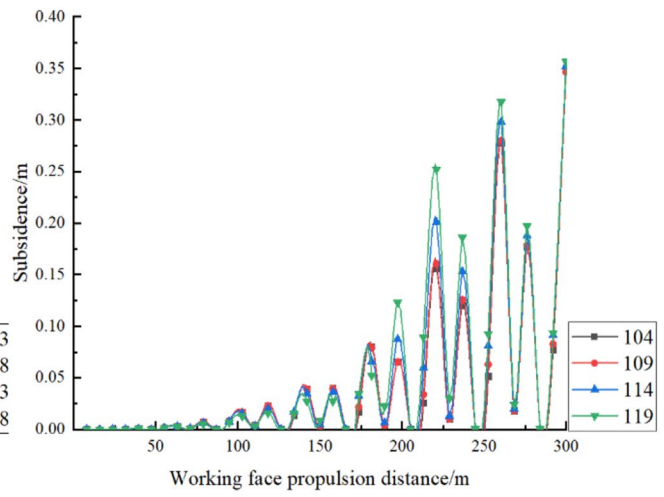
(1) Settlement when $X = 100$ m



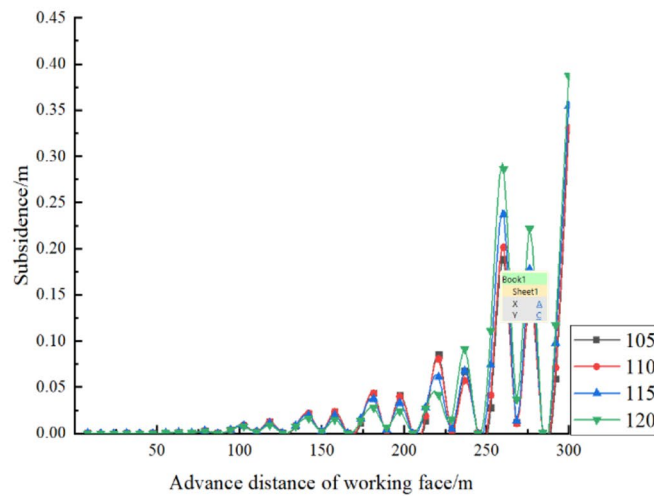
(2) Settlement when $X = 150$ m



(3) Settlement when $X = 200$ m



(4) Settlement when $X = 250$ m



(5) Settlement when $X = 300$ m

Fig. 11 Amount of subsidence at different advancing distances when unfilled

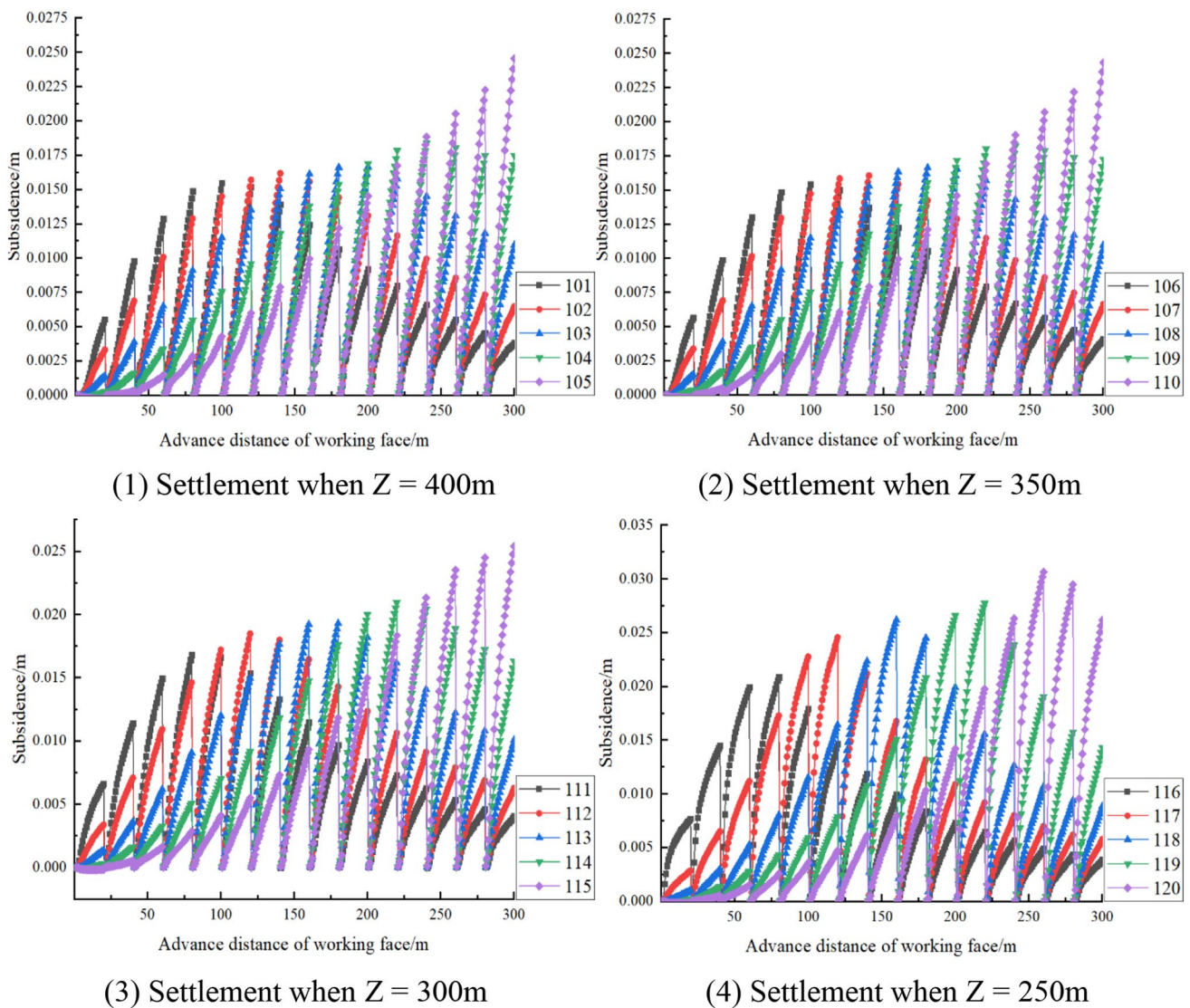


Fig. 12 Subsidence of each layer advanced with the working face during filling

positive direction gradually increases and almost no horizontal displacement in the negative direction occurs. This is because points 126–128 are located on the left side of the working face at 150 m, and points 129 and 130 are located on the right side of the working face at 150 m. In the mining process, points 126–128 are closer to the surface and points 129–130 are farther away from the surface, so they have less influence on points 129–130. By the same token, after advancing to 150 m, the influence on points 129–130 is greater.

According to Fig. 14(3), the displacement along the horizontal positive direction is larger at $Z = 300\text{ m}$, and the maximum displacement occurs when the working surface is advanced to 150 m. According to Fig. 14(4), it can be observed that the horizontal displacement is generally larger at closer to the mining position.

Based on the horizontal displacement data obtained for points 121–140, the horizontal displacement curves for different levels with the same horizontal coordinates are analyzed.

According to the overall analysis of Fig. 15, the following law was found. At $X = 100\text{ m}$, when the working surface advances to 150 m, the horizontal displacement of each level does not change much. When the working surface advances to 150 m, the displacement in the positive horizontal direction gradually increases. When $X = 150\text{ m}$, the displacement in the negative horizontal direction first increases and then decreases in front of the working surface advancing to 150 m. After advancing to 150 m, the displacement in the positive horizontal direction gradually increases. At $X = 200\text{ m}$, the horizontal displacement in the negative horizontal direction increases and then decreases

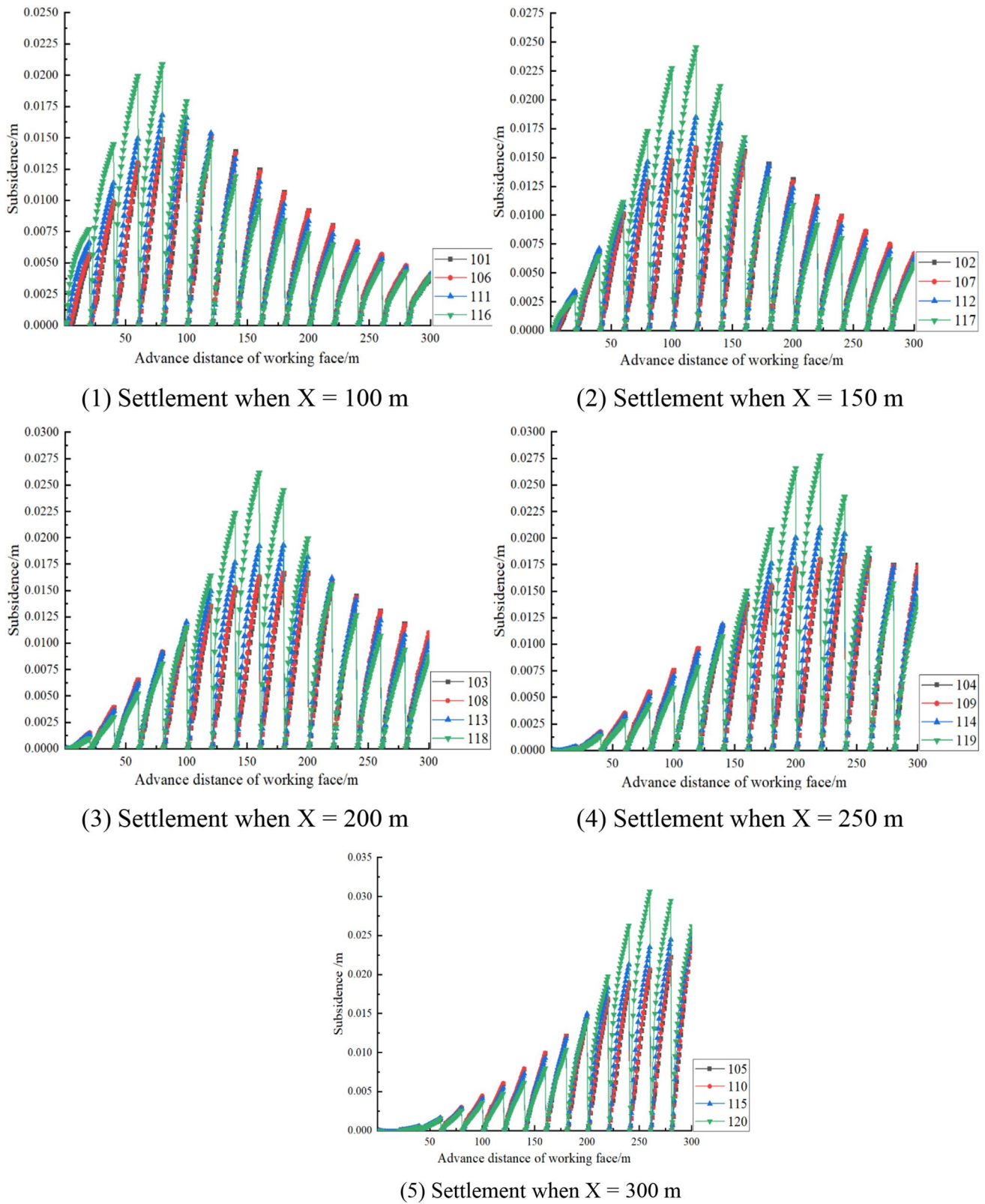


Fig. 13 Subsidence curve during filling

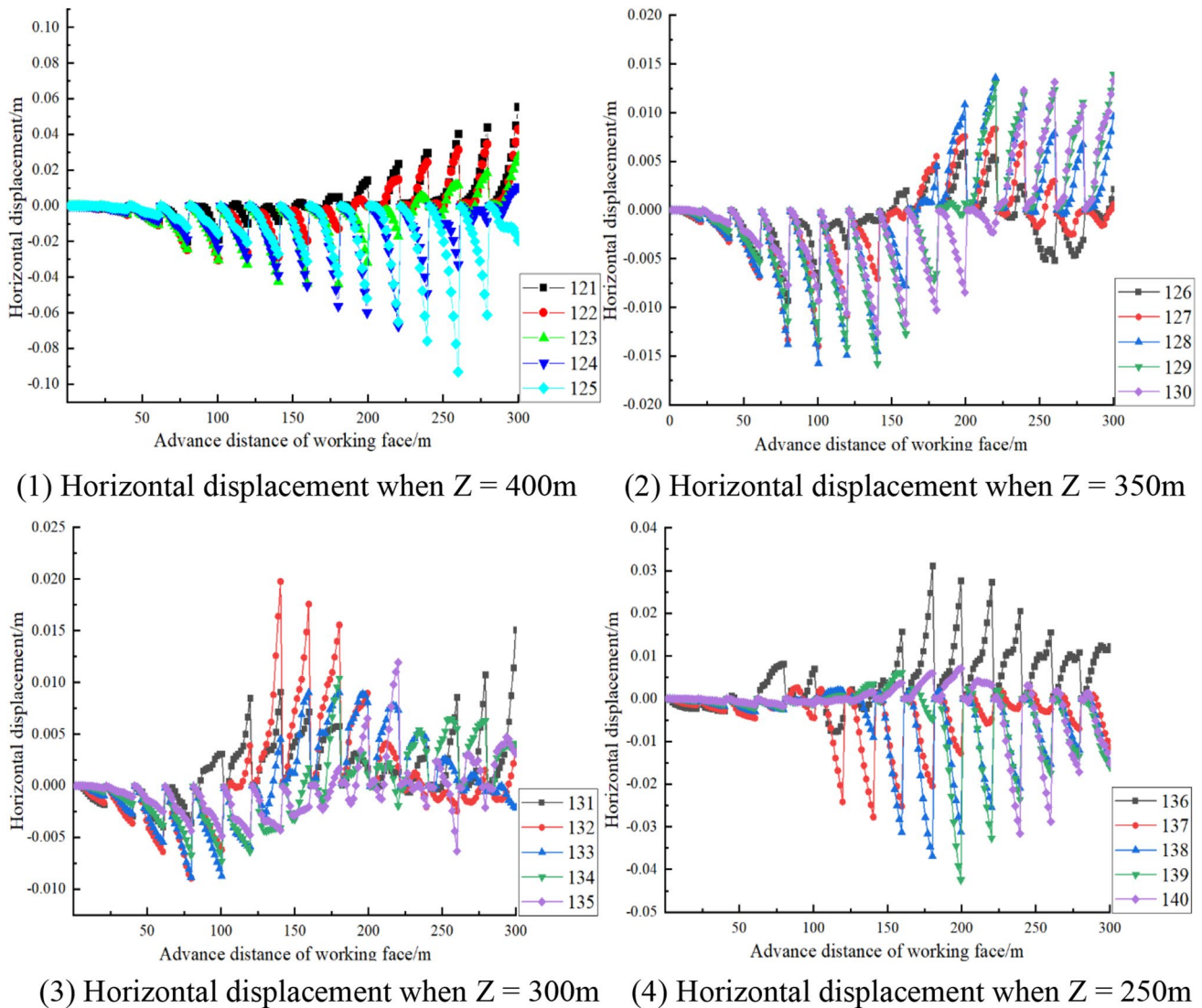


Fig. 14 Horizontal displacement of each layer when unfilled

as the working surface advances, and the maximum displacement occurs when the working surface advances to near 175 m. At $X = 250\text{ m}$ and $X = 300\text{ m}$, the law of displacement curve is similar to that at $X = 200\text{ m}$. In summary, it can be concluded that with the change of X , the maximum displacement gradually approaches to the value of X . The maximum displacement of the working surface is increased and then decreased.

The finite difference software FLAC3D was used to simulate the excavation of the ore body under mining-and-filling conditions, and the horizontal displacement curves at 121–140 points were obtained (Figs. 16, 17). According to Figs. 16 and 17, the horizontal displacement is reduced by about 10 times after the filling. The law of the horizontal displacement is similar to the unfilled one, but the trend of the curve tends to be flat. It can be concluded that the filling

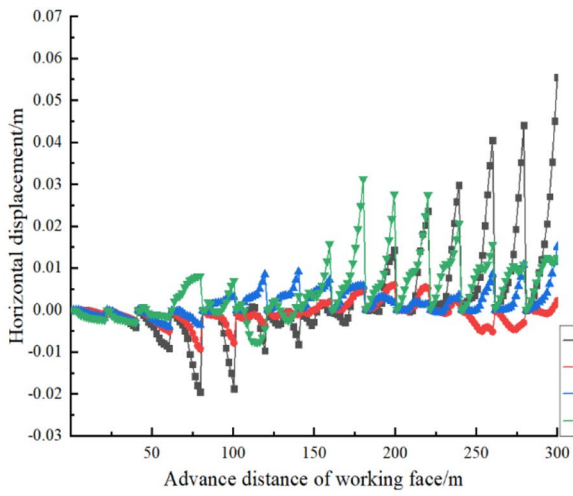
effectively reduces the damage of the horizontal displacement, and the filling effect is good.

The horizontal displacement curve of different horizons under the same filling conditions.

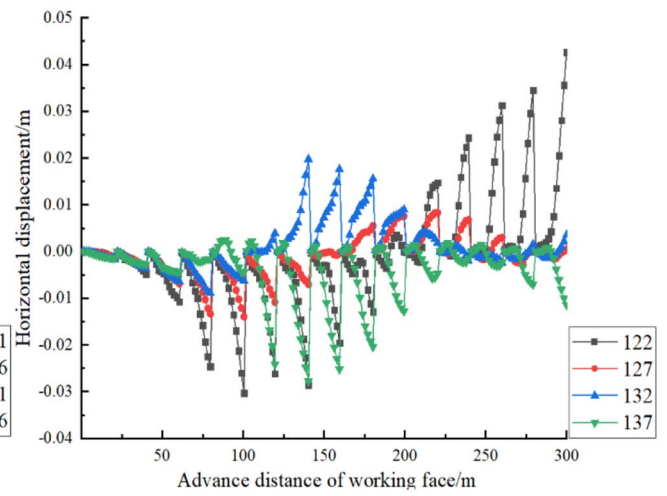
Plastic failure analysis

Plastic failure analysis without filling

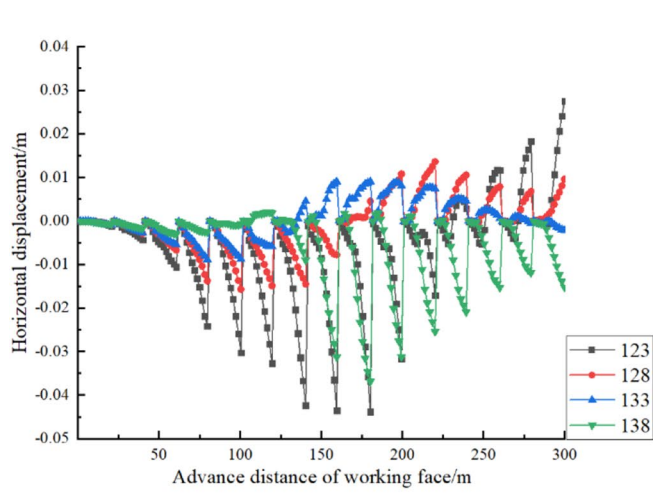
The finite difference software FLAC3D was used to simulate the excavation of the ore body under unfilled conditions, and the plastic zone failure cloud map was obtained (Fig. 18). According to the simulated plan design, one step is excavated every 20 m, for a total of 15 steps of 300 m. In order to fully observe and analyze the extent of plastic zone damage during the mining process, the plastic failure



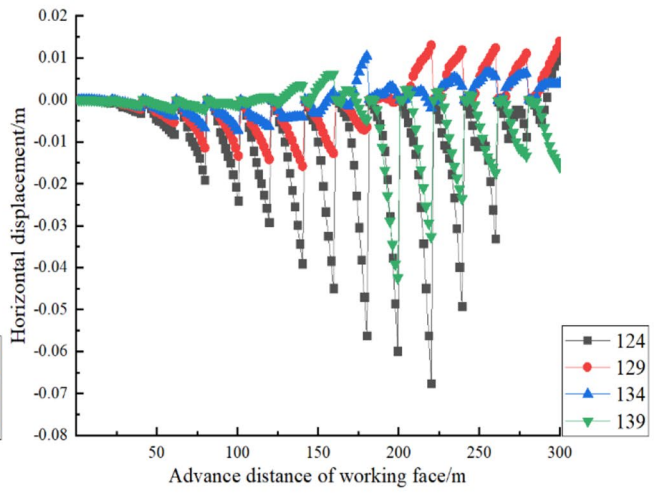
(1) Horizontal displacement when $X = 100$ m



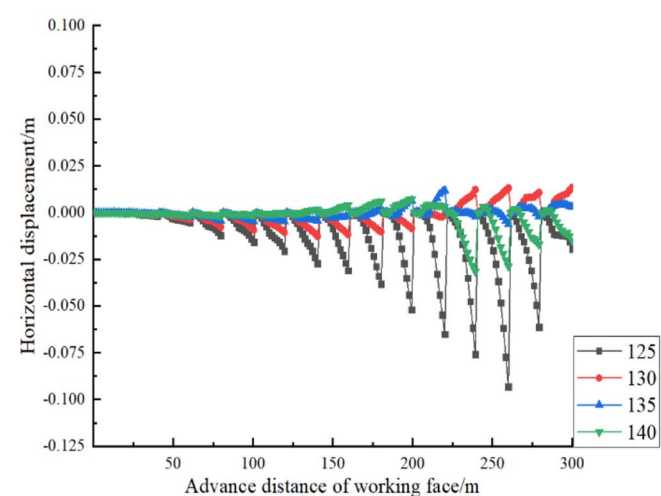
(2) Horizontal displacement when $X = 150$ m



(3) Horizontal displacement when $X = 200$ m

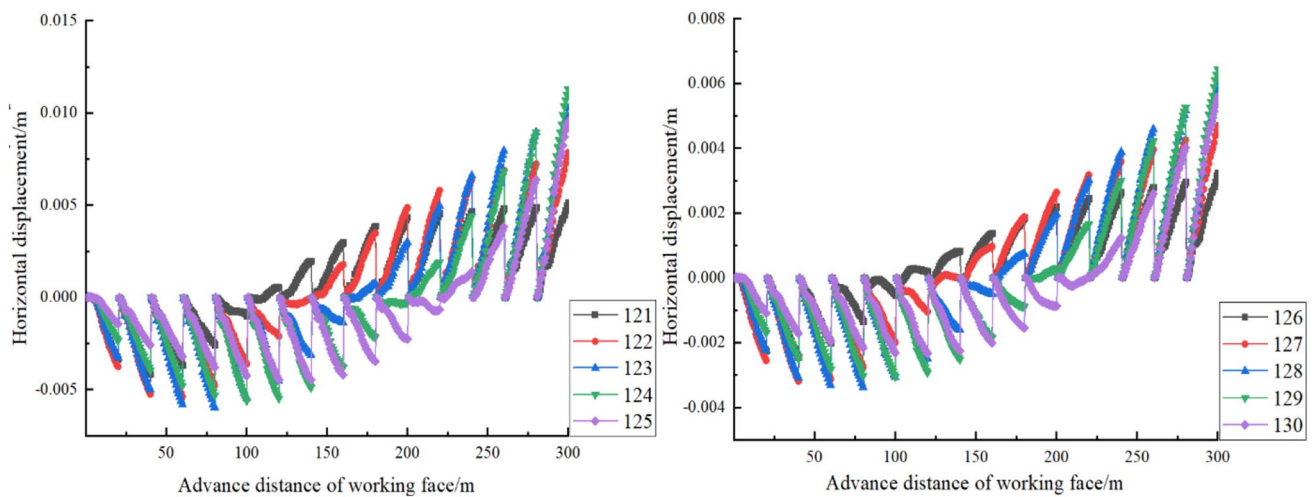


(4) Horizontal displacement when $X = 250$ m



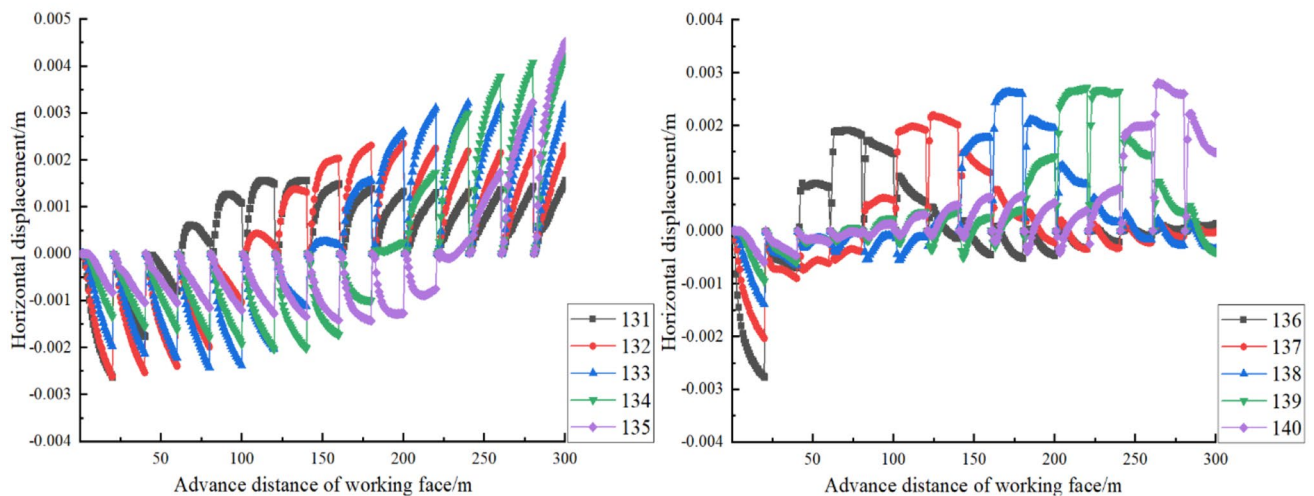
(5) Horizontal displacement when $X = 300$ m

Fig. 15 Horizontal displacement curves of different horizons when unfilled



(1) Horizontal displacement when $Z = 400\text{m}$

(2) Horizontal displacement when $Z = 350\text{m}$



(3) Horizontal displacement when $Z = 300\text{m}$

(4) Horizontal displacement when $Z = 250\text{m}$

Fig. 16 Horizontal displacement curves of different layers

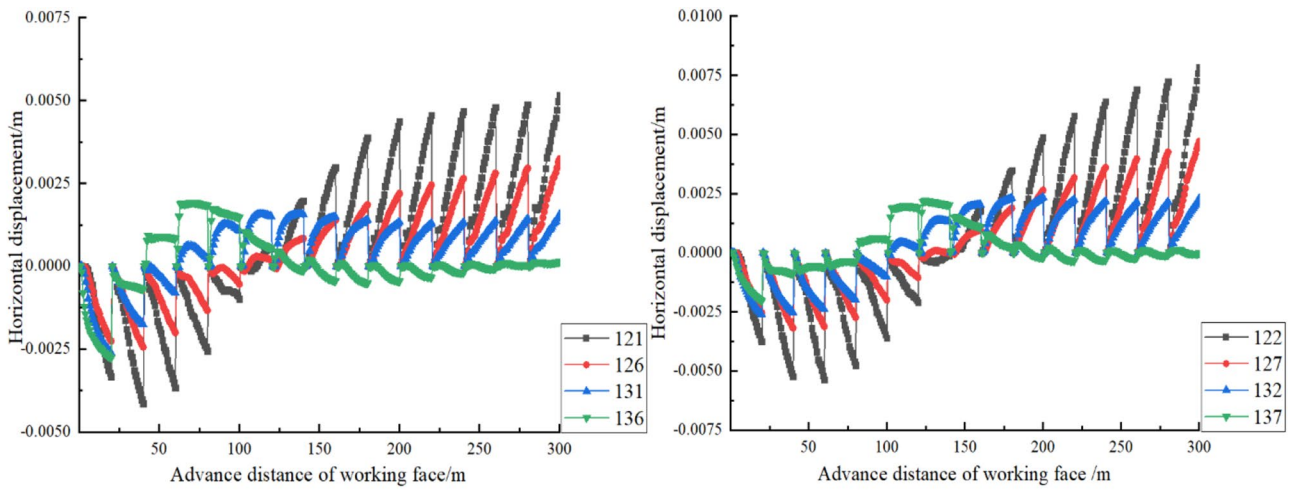
map of the whole process is displayed. Figure 18 shows that in the original rock state, the stratum is in equilibrium and no plastic failure is thought to have occurred. When the excavation is performed for 20 m, the plastic failure zone begins to appear. The main forms of plastic failure are compressional and tensile shear failure. As the face advances up to 180 m, the plastic failure reaches the surface, and as the face advances, the zone of plastic failure at the surface gradually increases. As the ore body is extracted, the plastic failure area increases rapidly, and a symmetrical “saddle-shaped” failure area appears directly above the mining part. When the ore body is mined up to 200 m, a “conical” damage zone appears directly underneath the mining site.

Plastic failure analysis during filling

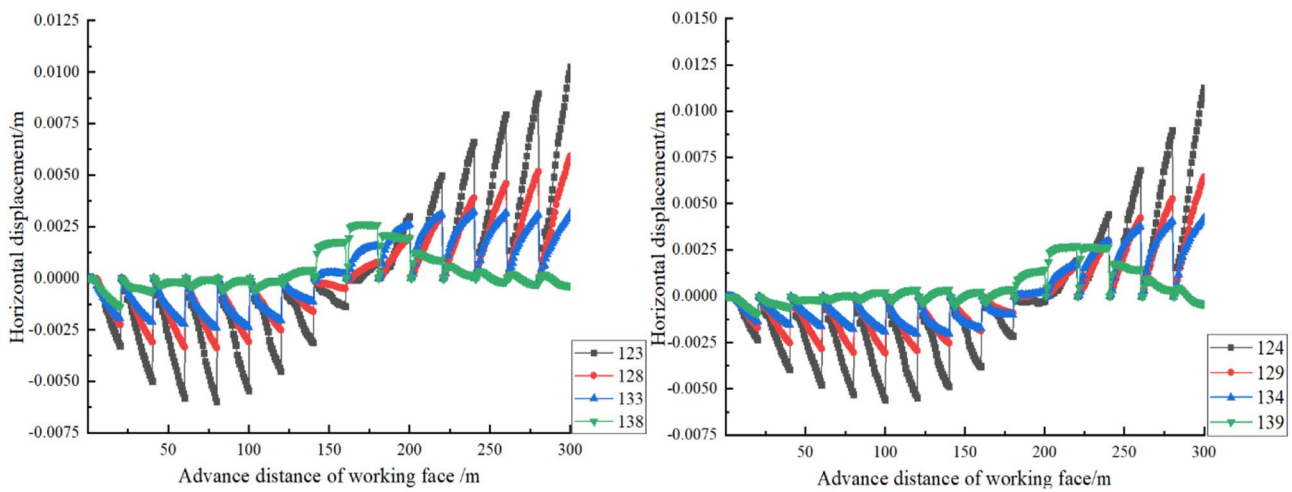
The finite difference software FLAC3D was used to simulate the excavation of the ore body under filling conditions, and the plastic zone damage cloud map was obtained (Fig. 19). According to Fig. 19, the plastic damage in the mined area after filling is mainly concentrated in the vicinity of the mining location and has almost no effect on the surface. Therefore, it can be concluded that the filling effectively reduces the plastic damage range.

Vertical stress analysis

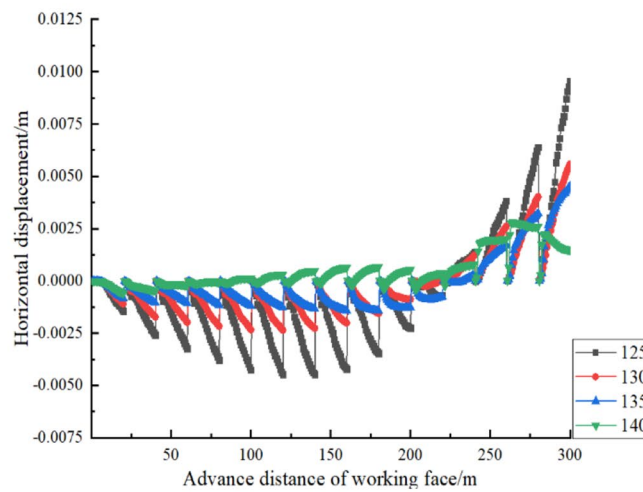
The finite difference software FLAC3D was used to perform excavation simulation of the ore body under unfilled



(1) Horizontal displacement when $X = 100$ m (2) Horizontal displacement when $X = 150$ m



(3) Horizontal displacement when $X = 200$ m (4) Horizontal displacement when $X = 250$ m



(5) Horizontal displacement when $X = 300$ m

Fig. 17 Horizontal displacement curve after filling

Fig. 18 Plastic failure cloud diagram without filling

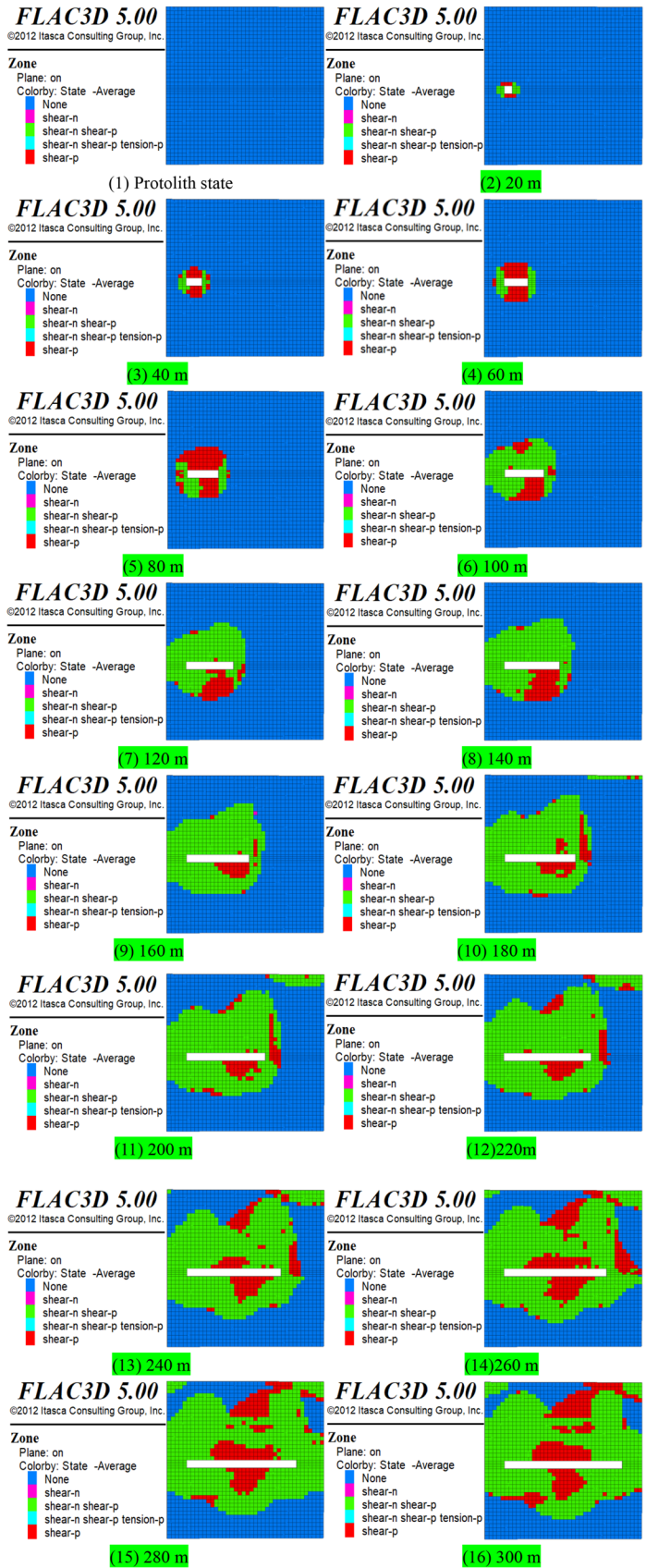


Fig. 18 Plastic failure cloud diagram without filling

Fig. 19 Plastic failure cloud diagram during filling

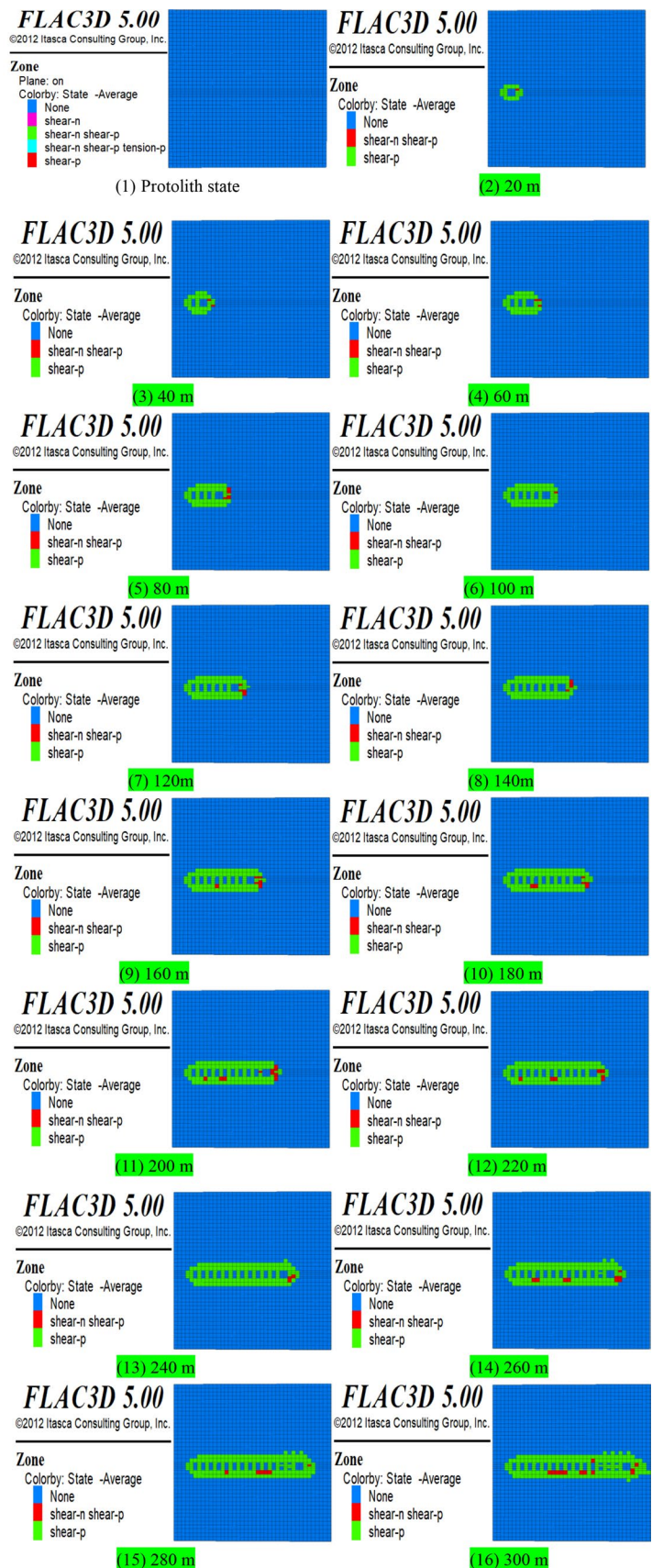


Fig. 20 Vertical stress cloud diagram without filling

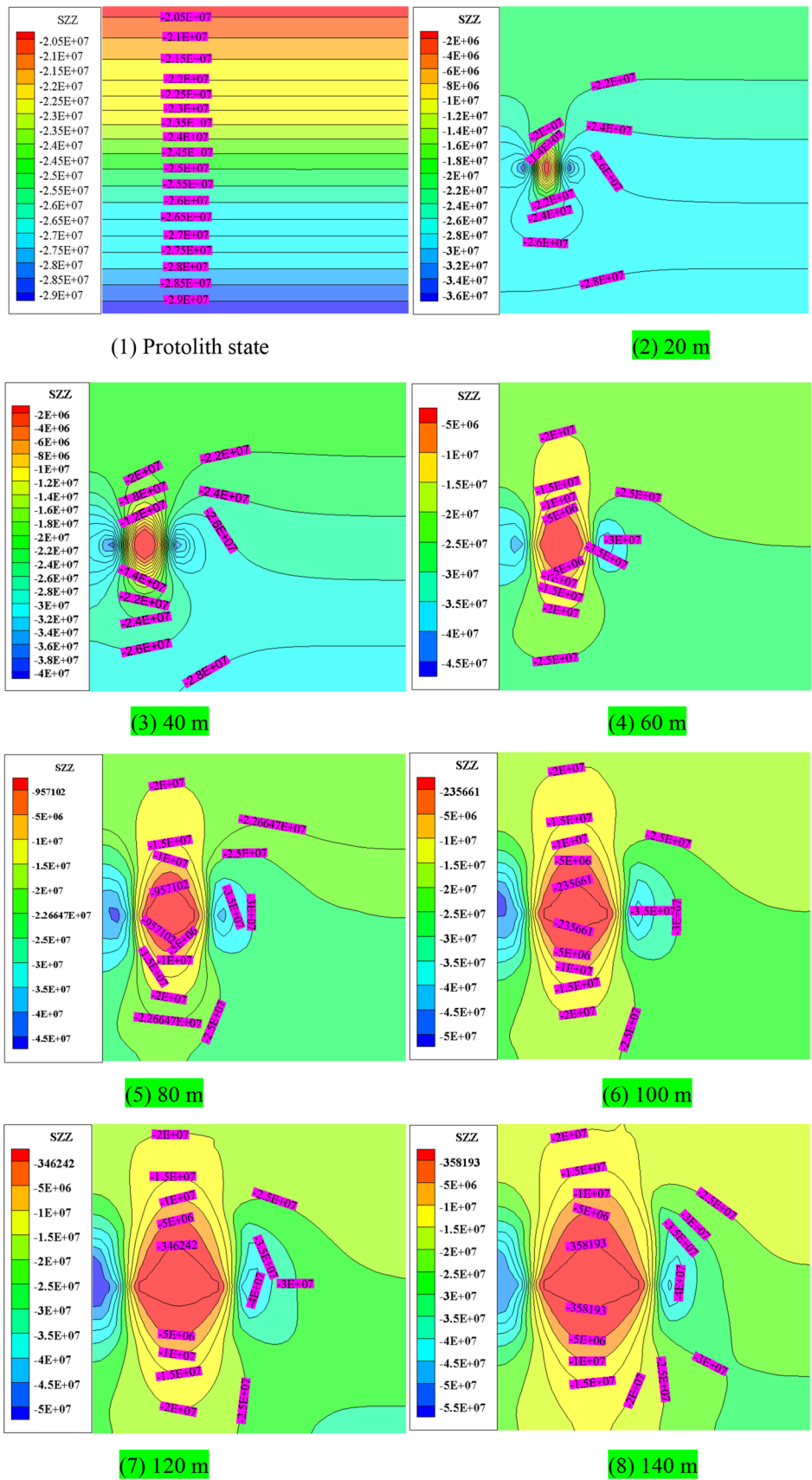
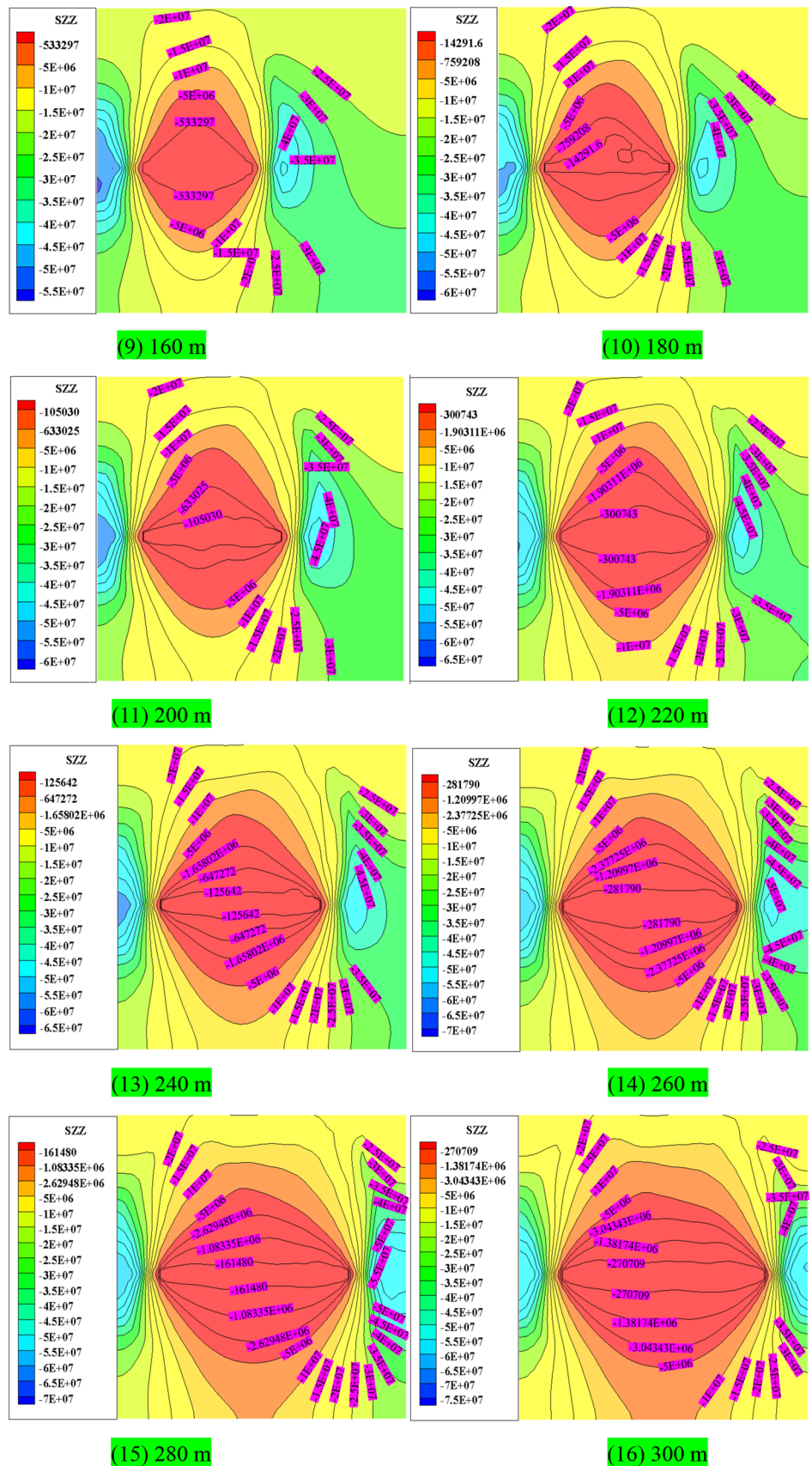


Fig. 20 (continued)



conditions to obtain the vertical stress curve (Fig. 20), and the excavation simulation of the ore body under filled conditions to obtain the vertical stress curve (Fig. 21).

Figure 20 shows that the maximum and minimum vertical stresses on the surrounding rock increase slowly after mining with tailings fill. The range of stress concentration in the vicinity of the cut hole decreases. As mining progresses, the vertical stress zone around the mining site increases slowly. The stress concentration zones in the mining area and in the attachment of the cutting eye change less. The vertical stress distribution around the mining site showed an irregular symmetrical pattern. The maximum vertical stress was 36 MPa, and the minimum vertical stress was 0.65 MPa.

The comparison between Figs. 20 and 21 shows that the vertical stress is greater in the open area before filling, and it tends to expand symmetrically with the excavation of the ore body. After filling the tailings, the maximum vertical stress is reduced from 43.7 to 36 MPa, and the vertical stress shows a slow increasing trend. Therefore, it is believed that the selected filling material can effectively reduce the stress concentration range and strength according to the ratio of tailings, material particle size, slump, lime–sand ratio and tailings settlement characteristics obtained from the experiment.

Mobile observatory analysis

In order to accurately monitor the surface settlement of the mined-out area of Laixin iron ore mine, a mobile observation station was used to measure the surface settlement in the mining area, which spanned the period from June 2017 to June 2018. According to the design principle of the mobile observatory, it was decided to set up two observation lines along the inclination of the ore body and one observation line towards the ore body, with 19 observation points on the inclination line 1, 19 observation points on the inclination line 2, and 25 observation points on the trend line (Fig. 22).

Points 1, 9, and 18 of the tendency line 1 were selected to draw a surface subsidence map (Fig. 23), points 5, 14, and 19 of the tendency line 2 were selected to draw a surface subsidence map (Fig. 24), and points 4, 14, and 21 of the tendency line 3 were selected to draw a surface subsidence map (Fig. 25).

From Fig. 23, we can see that the observation points on both sides of the mining site have less subsidence. The maximum subsidence at the beginning of mining is 35 mm, and the subsidence at the end of mining is larger than at the beginning. This means that the amount of subsidence at the surface will increase due to the effects of mining action. The maximum displacement subsidence of the observation point located at the center of mining is 75 mm, which indicates that the center of the surface movement basin is nearby.

From Fig. 24, we can see that in the new mining area, the surface subsidence pattern is consistent with Fig. 19, and the maximum surface subsidence amount does not change much.

From Fig. 25, the subsidence at the trend observation point is larger than that at the tendency observation point, which is caused by the larger distance in the trend direction.

Discussion

The construction of a geological model of surface subsidence is useful for the analysis of post-mining surface movement in mining areas, but it cannot be replicated on a large scale, because the model is built for specific geological conditions. The finite-difference software FLAC3D is used to simulate mining under filled and unfilled conditions, and the filling effect is reasonably evaluated with the amount of surface subsidence, horizontal displacement, plastic failure range of the surrounding rocks, and stress conditions on the surface and surrounding rocks as evaluation options. Based on the comparison between the simulation results and the actual observation results, the two basically fit together. However, it should be noted that due to the mechanical nature of the numerical simulation, it should be combined with the actual measurement in the actual application. The oscillation of the surface displacement curve in the thesis is caused by the limited selection of points and random errors.

Conclusion

1. Based on the knowledge of elastic mechanics, we established a subsidence model for insufficient mining and full mining, and predicted that the maximum subsidence value of the surface affected by mining occurs in the middle of the upper part of the emptied area. As the burial depth increases, the subsidence amount increases continuously.
2. Based on the finite difference software FLAC3D, a simplified three-dimensional numerical analysis model of Laixin Iron Mine was established, and numerical simulation was carried out by converting the tailings to fill the goaf and unfilled goaf. By analyzing the amount of subsidence, the amount of horizontal displacement, the plastic failure range of the surrounding rock, and the stress status of the surface and surrounding rock, it is found that the use of tailings filling can effectively reduce the amount of surface subsidence, the damage of the surrounding rock and the stress concentration.
3. The on-site mobile observation station is used to observe the surface subsidence, and the observation results are matched with the numerical simulation results, which verifies that the filling material data obtained from the

Fig. 21 Vertical stress cloud diagram during filling

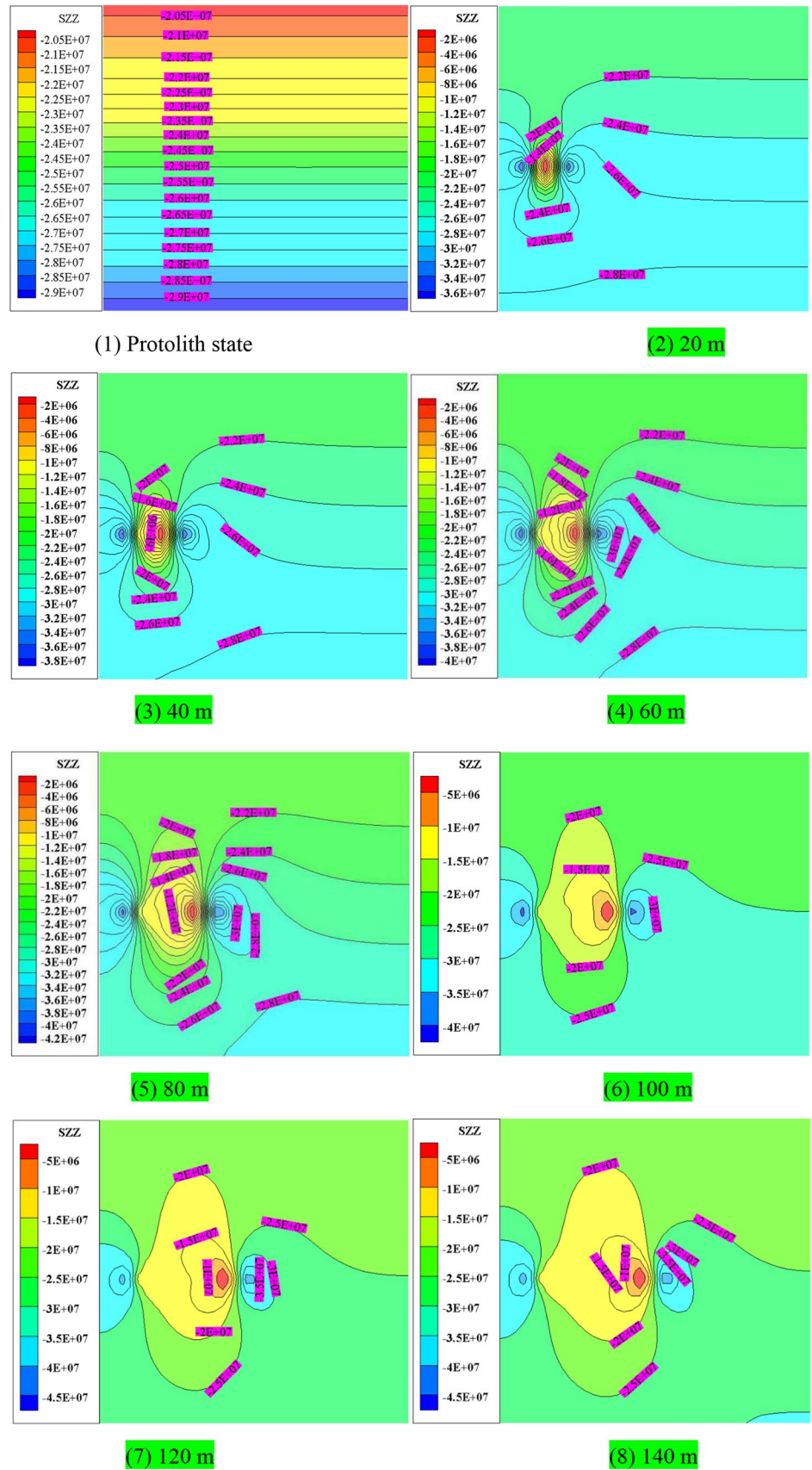
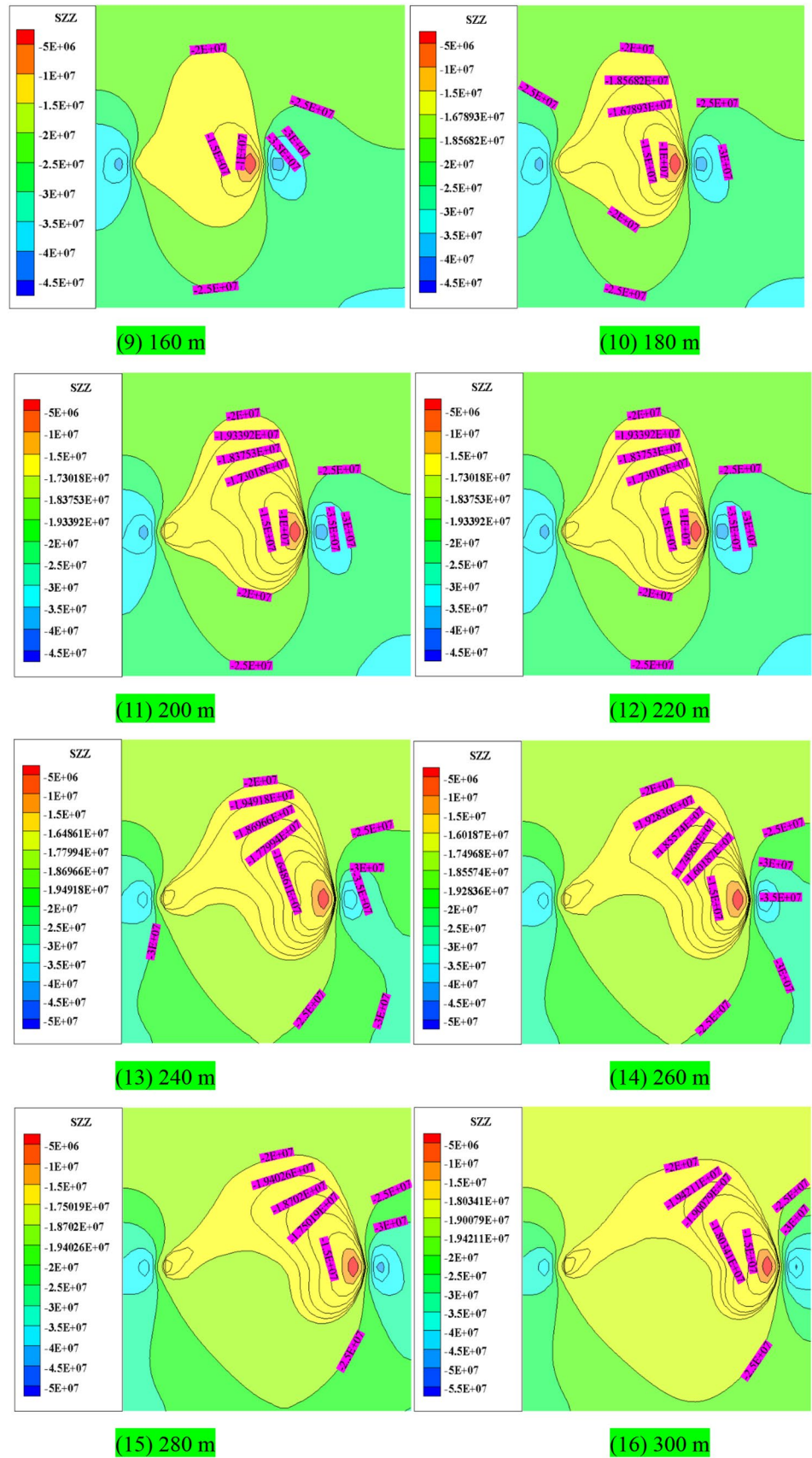


Fig. 21 (continued)



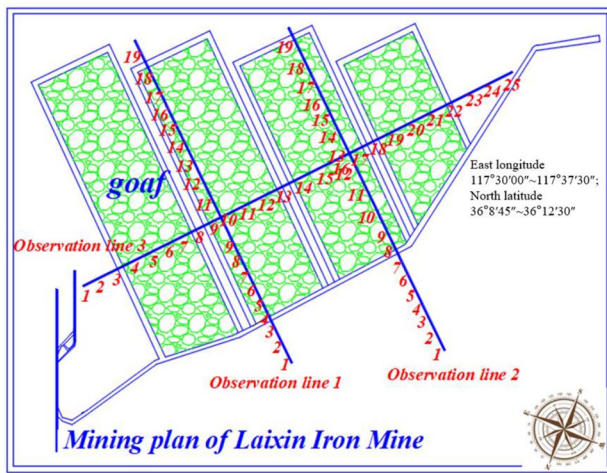


Fig. 22 Observation map of mining area

experiment is reliable, and also shows that the numerical simulation method can be used to predict the surface subsidence and displacement.

Fig. 23 Observation line 1 of inclined surface subsidence

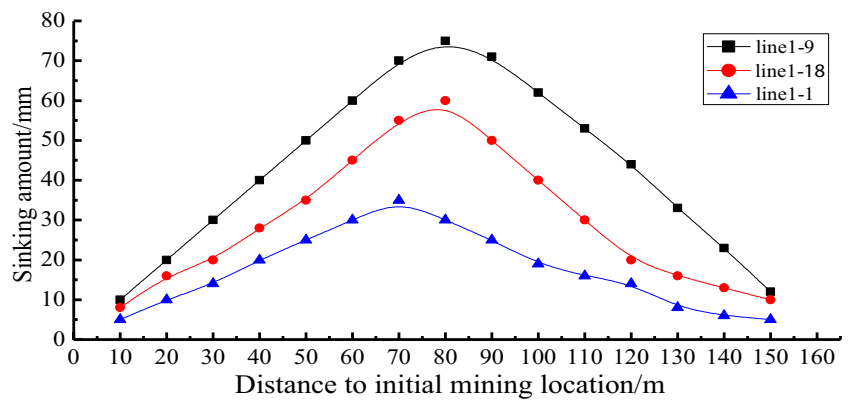


Fig. 24 Observation line 2 of inclined surface subsidence

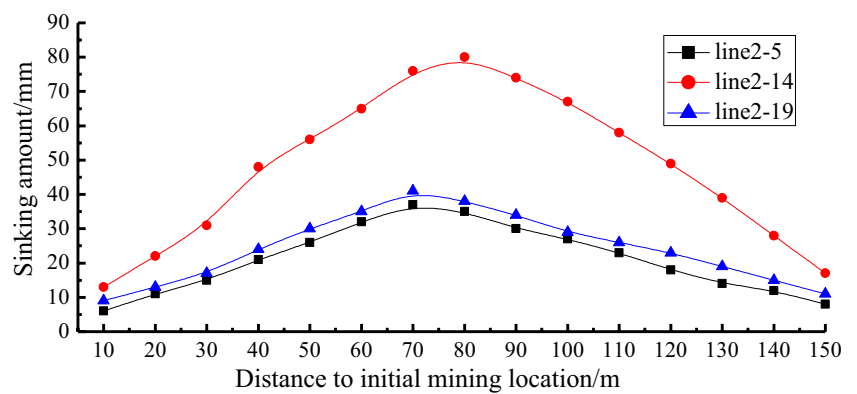
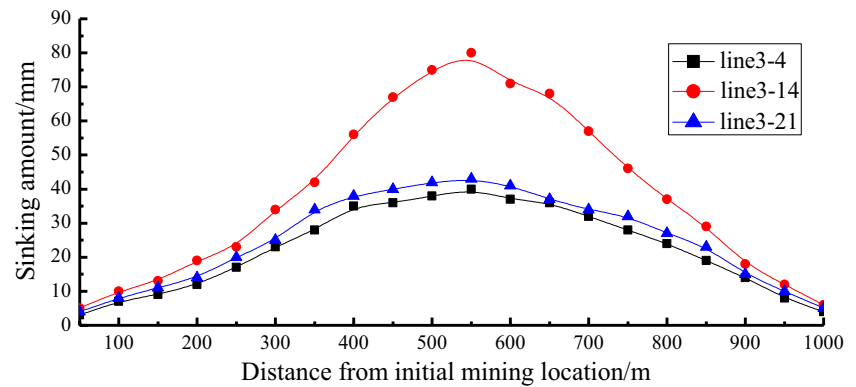


Fig. 25 Observation line 3 of surface subsidence along strike



Acknowledgements This research was funded by the National Natural science Foundation of China (Grant 51874192), the National High Technology Research and Development Program (863 Program) of China (Grant 2015AA016404-4), the Natural Science Foundation of Shandong Province (Grant ZR2019MEE084), the State Key Research and Development Program of China (Grant 2017YFC0804108), the Youth Program of National Natural Science Foundation of China (Grant 420071720) and the SDUST Research Fund (Grant 2018TDJH102).

Data availability The data used to support the findings of this study are available from the corresponding author upon request.

Declarations

Conflict of interest The authors declare that they have no conflicts of interest.

References

- Cai SJ, Huang G, Wu D, Zhang YD (2015) Experimental and modeling study on the rheological properties of tailings backfill. *J North-eastern Univ* 36(6):882–886
- Chaussard E, Kerosky S (2016) Characterization of Black sand mining activities and their environmental impacts in the Philippines using remote sensing. *Remote Sens* 8(2):100
- Chen QS, Zhang QL, Xiao CC, Chen X (2017) Backfilling behavior of a mixed aggregate based on construction waste and ultrafine tailings. *PLoS ONE* 12(6):e0179872
- Chen CL, Li XJ, Chen XD, Chai JH, Tian XH (2019) Development of cemented paste backfill based on the addition of three mineral additions using the mixture design modeling approach. *Constr Build Mater* 229:116919
- Dai HY, Wen-Chang LI, Liu YX, Jiang YD (2011) Numerical simulation of surface movement laws under different unconsolidated layers thickness. *Trans Nonferrous Metals Soc China* 21(supp S3):599–603
- Deng DQ, Liu L, Yao ZL, Song KI-IL, Lao DZ (2017) A practice of ultra-fine tailings disposal as filling material in a gold mine. *J Environ Manag* 196:100–109
- Emad MZ, Mitri H, Kelly C (2018) Dynamic model validation using blast vibration monitoring in mine backfill. *Int J Rock Mech Min Sci* 107:48–54
- Feng X, Zhang N, Gong L, Xue F, Zheng XG (2015) Application of a backfilling method in coal mining to realise an ecologically sensitive “black gold” industry. *Energies* 8(5):3628–3639
- Fokker PA, Visser K, Peters E, Kunakbayeva G, Muntendam-Bos AG (2012) Inversion of surface subsidence data to quantify reservoir compartmentalization: a field study. *J Pet Sci Eng* 96–97(10):10–21
- Fu JX, Du CF, Song WD (2014) Strength sensitivity and failure mechanism of full tailings cemented backfills. *J Univ Sci Technol Beijing* 36(9):1149–1157
- Juncosa R, Delgado J, Cereijo JL, Muñoz A (2019) Hydrochemical evolution of the filling of the mining lake of As Pontes (Spain). *Mine Water Environ* 38(3):556–565
- Lee SE, Park SJ, Kim HS, Jang HS, Kim TH (2012) A study on the model test for mine filling using coal ash. *터널과 지하공간 제 22권 제 6호 (통권 제 101호)* 22(6):449–461
- Li HL, Wang JP, Lan GJ, Huang HQ, Xie YB, Tang ZX, Pan HB (2014) Analysis and evaluation on the risk of karst collapse from the aspect of studying karst underground water—setting tanluo collapse in nanning as an example. *Shandong Land Res* 30(04):82–85
- Li HZ, Guo GL, Zha JF, Yuan YF, Zhao BC (2015) Research on the surface movement rules and prediction method of underground coal gasification. *Bull Eng Geol Environ* 75(3):1–10
- Li M, Zhang JX, Huang Y, Zhou N (2017) Effects of particle size of crushed gangue backfill materials on surface subsidence and its application under buildings. *Environ Earth Sci* 76(17):603
- Li J, Zhang SQ, Wang Q, Ni W, Li KQ, Fu PF (2020) Feasibility of using fly ash–slag-based binder for mine backfilling and its associated leaching risks. *J Hazard Mater* 400:123191
- Lin HW, Wang YP, Gao YL, Gao YL, Wang XL (2018) A filled function method for global optimization with inequality constraints. *Comput Appl Math* 37(2):1524–1536
- Lu B, Zhang XG, Li F, Zhang BL, Pang ZZ (2017) Study and application of short-wall gangue cemented backfilling technology. *Meitan Xuebao/J China Coal Soc* 42:7–15
- Ma Q, Tan YL, Liu XS, Gu QH, Li XB (2020) Effect of coal thicknesses on energy evolution characteristics of roof rock-coal-floor rock sandwich composite structure and its damage constitutive model. *Compos Part B Eng* 198:108086
- Ouattara D, Yahia A, Mbonimpa M, Belem T (2017) Effects of superplasticizer on rheological properties of cemented paste backfills. *Int J Mineral Process* 161(Complete):28–40
- Qi TY, Gao B (2013) Strata consolidation subsidence induced by metro tunneling in saturated soft clay strata. *J Modern Transport* 19(1):35–41
- Strozzi T, Delaloye R, Poffet D, Hansmann J, Loew S (2011) Surface subsidence and uplift above a headrace tunnel in metamorphic basement rocks of the Swiss Alps as detected by satellite SAR interferometry. *Remote Sens Environ* 115(6):1353–1360

- Strozzi T, Caduff R, Wegmüller U, Raetzo H, Hauser M (2017) Widespread surface subsidence measured with satellite SAR interferometry in the Swiss alpine range associated with the construction of the Gotthard Base Tunnel. *Remote Sens Environ* 190:1–12
- Sun W, Zhang Q, Luan YZ, Zhang XP (2018) A study of surface subsidence and coal pillar safety for strip mining in a deep mine. *Environ Earth Sci* 77(17):627
- Villegas T, Nordlund E, Dahnér-Lindqvist C (2011) Hangingwall surface subsidence at the Kiirunavaara Mine, Sweden. *Eng Geol Amst* 121(1–2):18–27
- Wang BL, Xu JL, Xuan DY (2018) Time function model of dynamic surface subsidence assessment of grout-injected overburden of a coal mine. *Int J Rock Mech Min Sci* 104:1–8
- Yin SH, Shao YJ, Wu AX, Wang YM, Chen X (2018) Expansion and strength properties of cemented backfill using sulphidic mill tailings. *Constr Build Mater* 165:138–148

Publisher's Note Springer Nature remains neutral with regard to jurisdictional claims in published maps and institutional affiliations.